Characterization of retention and separation mechanisms with Pirkle-type enantioselective stationary phases in supercritical fluid chromatography

Caroline West, Syame Khater

Characterization of retention and separation mechanisms with Pirkle-type enantioselective stationary phases in supercritical fluid chromatography

Caroline West *[1], Syame Khater[1]

1. Univ Orleans, CNRS, Institut de Chimie Organique et Analytique (ICOA), UMR 7311, B.P. 6759, rue de Chartres, F-45067 Orléans cedex 2, France.

Corresponding author:
Tel.: (+33)238 494 778
caroline.west@univ-orleans.fr

Abstract

In the present study, we characterize a famous Pirkle-type enantioselective stationary phase ((R,R)-Whelk-O1 from Regis Technologies) and an equivalent enantiomeric phase (ReproSil Chiral-NR from Dr. Maisch) in supercritical fluid chromatography (SFC) with carbon dioxide – methanol (90:10 v/v) mobile phase. First, the interactions contributing to retention are evaluated with a modified version of the solvation parameter model, comprising five Abraham descriptors (E, S, A, B, V), two additional descriptors to take account of molecular shape (flexibility F and globularity G), and two additional descriptors to take account of interactions with ionizable species (D^- and D^+). Linear solvation energy relationships (LSER) are established based on the retention of 212 achiral analytes. As expected, π-π interactions are the most significant to explain retention, while dipole-dipole, hydrogen bonding and ionic interactions with cationic species are of secondary importance.

Secondly, the contributions of interactions to enantioseparations are discussed, based on the analysis of 79 racemates. Discriminant analyses (DA) were computed to gain some insight on retention mechanisms. The set of racemates is first divided between racemates eluted earlier than expected based on the LSER models, and those eluted later than expected. Small spherical molecules are more retained than expected, as they may better fit inside the cleft of the chiral selector. They are also most frequently resolved, probably for the same reason. Among the molecules that are less retained than expected, which are rather large and/or non-spherical, other features are favourable to enantiorecognition: π-electrons, dipoles and electron-donating properties. Contrary to the observations on other sorts of chiral selectors, flexibility was found to have no contribution on the enantiorecognition process.

Keywords: chiral stationary phases; discriminant analysis; enantioseparation mechanisms; Pirkle-type phases; solvation parameter model; supercritical fluid chromatography.

1. Introduction

Brush-type chiral stationary phases (CSPs) [1] were among the first chiral selectors purposely designed for liquid-phase chromatographic resolution of enantiomers. Previously, naturally occurring chiral selectors like proteins [2] or amino acids (particularly for ligand-exchange chromatography [3]) had been immobilized on silica supporting phases for use in enantioselective liquid chromatography. Brush-type CSPs with charge-neutral synthetic selectors were initially developed by William H. Pirkle and co-workers from the end of the 1970s [4,5], which is why these phases are often named “Pirkle-type”. The idea behind the ligands proposed was to offer three points of interaction that would comply with the “three-point attachment model” initially proposed by Easson and Stedman for protein binding [6], and later adapted for enantioselective chromatography by Dalgliesh [7]. Although not entirely accurate in describing the enantioseparation process, it is still convenient to design such chiral selectors based on this model. As appears with the example in Figure 1, the chiral ligands are designed to have three (or more) different interaction points. However, what does not appear on this figure is that the bulky ligands also have a well-defined, rather rigid spatial arrangement [8–10], with the tetrahydrophenanthrene ring and the dinitrobenzyl ring being positioned in an orthogonal fashion, thereby forming a cleft. The dinitrobenzyl group appears to be the only one with some conformational flexibility, somewhat rotating to bind the analytes inside or outside the cleft [8,10]. As a result, chiral discrimination is favoured when steric fit occurs, that is to say when the enantiomers have the adequate size, shape and three-dimensional organization of the interacting groups to fit in the chiral cleft of the ligand [5,11]. Three-dimensional structures have been shown in the past, based on crystallographic measurements [11] or based on molecular modelling [8–10].

Compared to other CSPs that are now frequently used like polysaccharides [12–14], macrocyclic glycopeptides [15–17] or protein-based phases [2], one advantage of such brush-type phases is that the ligand has a controlled chiral configuration, and an enantiomeric form may exist with the opposite configuration. For instance, the most famous Whelk-O1 stationary phase designed by Pirkle and Welch [18] can be found in (R,R) configuration (as in Figure 1) or in (S,S) configuration, thereby offering the possibility to control the elution order of enantiomers by choosing one chiral selector or its enantiomeric form. Indeed, when the aim of the chiral separation is to measure an enantiomeric excess, the minor enantiomer should preferably elute first to avoid being masked by the tailing peak of the major enantiomer. On the contrary, when purification is desired, the preferred enantiomer (whichever its proportion) should elute first because the first peak purified is usually obtained with a higher purity than the second. Indeed, although their loadability is not

as high as that of polysaccharide CSPs, it is still higher than the loadability of CSPs based on proteins, cyclodextrins and macrocyclic glycopeptides [19], making Pirkle-type CSPs useful for preparative purposes. Stereoismer identification and measuring extreme enantiomeric excess values (>99%) can be enabled by the possibility to reverse the stereoisomers elution order with chiral selectors of opposite configuration, as was demonstrated with the “Inverted Chirality Columns Approach” proposed by Gasparrini and co-workers [20–22].

Following the current trend of reducing particle size, the most recent version of Whelk-O1 for analytical-scale separations is available on sub-2 µm fully porous particles and has demonstrated improved efficiencies, as could be expected [23,24].

While Pirkle-type stationary phases were mostly employed in high-performance liquid chromatography (HPLC), they are also useful in supercritical fluid chromatography (SFC), where they are usually found to offer complementary capabilities for enantioselectivity to the most employed polysaccharide CSPs [25]. In this field, the Whelk-O1 phase appears as the most widely distributed brush-type phase. Modern SFC is essentially based on the use of pressurized carbon dioxide as the principal component of the mobile phase, together with a co-solvent (most often a short-chain alcohol) [26,27]. Thanks to several interesting attributes of carbon dioxide (low toxicity, no safety issues, low price) and the inherent advantages of the technique (low-viscosity fluid and high diffusivities providing high efficiencies even at high flow rates, low amount of waste especially after preparative separations), SFC has long been a favourite to achieve enantioseparations [28,29], usually offering higher resolution per unit time than enantioselective HPLC, thanks to high efficiency and high flow rate [30,31].

In previous works, we have proposed a chemometrics strategy to improve understanding of SFC enantioseparation mechanisms based on the use of linear solvation energy relationships (LSER) and discriminant analyses (DA) [32,33]. First, we developed a modified version of the solvation parameter model, comprising five Abraham descriptors (E, S, A, B, V) and four additional descriptors that were introduced to bring complementary information related to (i) analyte shape features of flexibility (F) and sphericity (or globularity, G) and (ii) ionic interaction capability through anionic (D^-) and cationic (D^+) analyte properties. With this model, we have previously examined polysaccharide CSPs [34,35], macrocyclic glycopeptide CSPs [36,37] and *Cinchona*-based brush-type CSPs [38], all in SFC conditions. In the present paper, this modified solvation parameter model is employed to characterize the (R,R)-Whelk-O1 enantioselective stationary phase in supercritical fluid chromatography based on the analysis of 212 achiral analytes. A similar phase from a different manufacturer (ReproSil Chiral-NR), carrying the (S,S) enantiomeric ligand from (R,R)-Whelk-O1 was included for comparison purposes, as we had observed in the past that

supposedly identical enantioselective stationary phases provided by different manufacturers could sometimes be significantly different [39].

Secondly, we have also demonstrated earlier that discriminant analysis (DA) was a useful tool to unravel the contributions of analyte features to enantiorecognition [34–36]. Based on the analysis of 79 chiral analytes, the structural features contributing to favourable enantiorecognition of (R,R)Whelk-O1 in SFC will be discussed.

3. Material and methods

3.1. Stationary phases

The stationary phases used in this study are commercially available: (R,R)-Whelk-O1 from Regis Technologies was packed in 150 x 4.6 mm column, with fully porous 5 µm silica particles, and ReproSil Chiral-NR (bonded with the (S,S) ligand) from Dr. Maisch was packed 250 x 4.6 mm column, with fully porous 8 µm silica particles.

3.2. Chemicals

The solvent used was HPLC-grade methanol (MeOH) provided by VWR (Fontenay-sous-Bois, France). Carbon dioxide of industrial grade 99.5% was provided by Air Liquide (France). 212 achiral test compounds (Table S1 in supplementary information) were obtained from a range of suppliers and were used to evaluate the contributions of molecular features to retention through LSER. 79 chiral racemic test compounds (Table S2 in supplementary information) were used to evaluate the contributions of molecular features to enantiorecognition through DA.

3.3. Chromatographic system and conditions

Chromatographic separations were carried out using equipment manufactured by Jasco (Tokyo, Japan). Two model 980-PU pumps were used, one for carbon dioxide and a second for the modifier. Control of the mobile phase composition was performed by the modifier pump. The pump head used for pumping the carbon dioxide was cooled to –5 °C by a cryostat (Julabo F10c, Seelbach, Germany). When the two solvents (methanol and CO_2) were mixed, the fluid was introduced into a dynamic mixing chamber PU 4046 (Pye Unicam,

Cambridge, UK) connected to a pulsation damper (Sedere, Orleans, France). The columns were thermostated by an oven (Jetstream 2 Plus, Hewlett-Packard, Palo Alto, USA), regulated by a cryostat (Haake D8 GH, Karlsruhe, Germany). The detector was a Gilson UV 151 detector (provided by Waters, Milford, MA) equipped with a pressure-resistant cell. After the detector, the outlet column pressure was controlled by a Jasco BP-2080 Plus pressure regulator. The outlet regulator tube (internal diameter 0.25 mm) was heated to 60 °C to avoid ice formation during the CO2 depressurization. The UV detection wavelength was 210 nm. Chromatograms were recorded using the Azur software (Datalys, France).

The mobile phase used in this study is always CO_2-MeOH 90:10 (v/v) without any additive. Flow rate was 3 mL min^{-1}. The oven temperature was set at 25°C and the outlet pressure was maintained at 15 MPa. Strictly speaking, the fluid is thus not supercritical but could be called subcritical. No distinction will be made in the following.

3.4. Data analysis

The Abraham solute descriptors (E, S, A, B, V) used for LSERs with Eq. (1) were extracted from an in-house database established from all available literature on the solvation parameter model (Tables S1 and S2). The two additional descriptors for charges (D^- and D^+) were calculated based on aqueous pK_a values determined with Chemicalize program and apparent pH 5. See previous works for detailed description [40]. The additional descriptors for flexibility (F) and globularity (G) were computed as previously described [32,33].

Multiple linear regressions (MLR) and discriminant analysis (DA) were performed using XLStat 19.03.44850 software (Addinsoft, New York, NY). The quality of the MLR fits was estimated using the adjusted determination coefficient (R^2), standard error in the estimate (*SE*) and Fisher *F* statistic. The statistical significance of individual coefficients was evaluated with the 95% confidence intervals.

The quality of DA was estimated based on ROC (receiver operating characteristics) curves and confusion matrices (see Figure S1 in supplementary information).

4. Results and discussion

The stationary phases examined in this paper bear the same chiral selector (in two enantiomeric forms), presented in Figure 1. The ligand can be fragmented into three sections: two aromatic rings arranged in a perpendicular orientation, with one being π-donor (the tetrahydrophenanthren ring) and the other one being both a π-acceptor, a dipole-dipole

interaction site and a hydrogen bond acceptor site (the 3,5-dinitrobenzoyl ring); between them is an amide function acting as a hydrogen-bond system, which can contribute to hydrogen bonding both as a proton donor (-NH- group) and as a proton acceptor (C=O group). This stationary phase is one of those of which the recognition mechanism has been described with most details [4] and is supposedly one of the easiest to explain (unlike the most complex CSPs based on polysaccharide of macrocyclic glycopeptides). Many of the molecular modelling studies to date were down with the chiral selector placed in a supposed "gas state" (not considering possible mobile phase components) [41], or sometimes in a "liquid state" (considering solvent molecules) [9], and always compared the computational results to liquid chromatography experimental data. In papers from Cann and co-workers relating docking studies [9,10], four interaction modes (M1-M4) were observed to occur between the analytes and the chiral selector. The latter was mostly in one, energetically more stable conformation, but could adopt a slightly different conformation for one interaction mode (M1 "side-of-cleft binding"), with the dinitrophenyl group rotating in a perpendicular position. It was also shown that predicting the outcome of a separation on this stationary phase was possible, with rather high success rate of the prediction [42], which is another indication of a well-defined enantiorecognition process. Comparison to the knowledge previously acquired with molecular modelling and liquid chromatography, to our results, based on a statistical model and observations done in pressurized carbon dioxide – methanol mobile phase, was also of interest in this study.

The sets of achiral and chiral probe analytes were previously designed for the characterization of polysaccharide CSPs. It is worth mentioning that it is still adequate to characterize these brush-type CSPs as appears from Figure 2.

First, the retention data of the achiral analytes (Table S1) are adequately scattered in a wide retention space with log *k* values ranging from -1 to +2 (Figure 2a). Besides, the retention data between the two columns were highly correlated (R^2 = 0.97), but the slope of the correlation line was significantly inferior to 1 (0.80) indicating that the two columns have *homeoenergetic* behaviour, according to the definition proposed by Horváth and co-workers [43], and suggesting similar physico-chemical basis for retention on the two columns. The κ-κ plot (log *k* vs. log *k*) can be observed in Figure S2 provided in supplementary information. The observed slope inferior to 1 may simply result from the different silica particles employed to support the chiral selector. Full information on the silica (pore size, specific surface area) and bonding density was not available, but the two CSPs had different particle size (5 and 8 µm).

Secondly, the separation data measured for the analytes in Table S2 are also adequately scattered with log α values ranging from 0 to 0.4 (Figure 2b) and about 60% showing α values >1. For the purpose of identifying the structural features contributing to

enantiorecognition, it is important that the probe set comprises both resolved and non-resolved enantiomers.

4.1. Interactions contributing to retention

The LSER equation employed in this work was previously described [37]:

$$\log k = c + eE + sS + aA + bB + vV + d^{-}D^{-} + d^{+}D^{+} + fF + gG \quad (1)$$

Briefly, the capital letters are molecular descriptors: E is related to the presence of π and n electrons, S is related to the presence of dipoles, A is related to proton-donor capability, B is related to electron-donor capability, V is the molecular volume, D^- is the total negative charge, D^+ is the total positive charge, F qualifies the molecule flexibility and G is the molecule sphericity. The small case letters are the system constants obtained from multiple linear regression of retention data (log *k* values) for a large set of analytes with known descriptor values. They quantify the relative contribution of interactions to the retention mechanism.

The results of LSER characterization are presented in Figure 3 (normalized coefficients), with complete data and statistics available in Table 1. The statistics were reasonably good, with R^2_{adj} values of about 0.85 and standard deviation in the estimate of 0.28 and 0.14 for Whelk-O1 and ReproSil Chiral-NR respectively. These results are clearly not as good as is usually observed when the solvation parameter model is applied for achiral separations, whatever the chromatographic mode, but considering the complexity of the system used here, they should be good enough to interpret the contributions of interactions to retention. The two columns yielded identical models as no significant difference can be observed (considering standard error bars). This is in accordance with the previous observation of high correlation of the retention data (Figure S2).

A first observation is that the *e* term, reflecting interactions associated to the presence of π and n electrons in the analytes, is by far the most significant one to contribute to retention. This was naturally expected, judging from the two aromatic groups (dinitrobenzyl and tetrahydrophenanthryl) in the chiral selector. Halogen bond [44], occurring between halogen atoms of some probe analytes and the nitrogen and oxygen atoms or π-donor system of the chiral selector may also be included in this *e* term. Typically, retention increase is observed when moving from chloride to bromide and iodide. For instance, this can be observed with halogenobenzenes (analytes #87 to #89 in Table S1) and halogenonaphthalenes (analytes #96 to #98).

Next to the *e* term, hydrogen bonding interactions with proton donors (*a* term) and acceptors (*b* term) are the most significant, and are related to the presence of the amide function in the chiral selector, which can interact both with proton donors (*a* term) and proton acceptors (*b* term), but also to the presence of nitro groups that can interact with proton donors [8–10,45].The influence of hydrogen bonding can be observed for instance in the increased retention observed when increasing the number of hydroxyl groups in the analyte, as for phenol, resorcinol and phloroglucinol (analytes #103, 108 and 111 in Table S1), or for any pair of analytes differing from one hydroxyl group (many possible pairs in Table S1).

Of slightly inferior significance are the dipole-dipole interactions (*s* term) related to the amide and nitro functions, and the interactions with cationic species (d^+ term), possibly due to non-bonded silanol groups at the surface of the silica supporting phase. The latter would also cause some repulsion to anionic species, as appears from the negative d^- term. Another possible contribution to the retention of ionic analytes is through the aromatic groups of the chiral selector. Firstly, the nitro functions carry partial negative charges on the oxygen atoms, which could also be responsible for the attraction of cationic analytes and repulsion of anionic analytes. Secondly, the tetrahydrophenanthrene ring is a π-donor system, which could also interact with electron-deficient cationic analytes and be responsible for the positive d^+ term. It is also worth mentioning that the d^-/d^+ terms are not significantly different between the two stationary phases, suggesting that silanol accessibility and/or ligand bonding density should be comparable between the two phases.

From these models, analyte size (described by the V descriptor) appears to have no influence on analyte retention. However, the analyte shape described by the G descriptor is significant: spherical molecules (large G values) must be somewhat sterically excluded from the stationary phase, as opposed to flat and/or linear molecules (small G values). Significant examples can be observed with polynuclear aromatic hydrocarbons. For instance, *p*-terphenyl (analyte #180 in Table S1), a rod-like molecule, is more retained than *o*-terphenyl (analyte #179) which is more spherical, as indicated by a larger G value. These observations may be somewhat contradicted because there is some inter-correlation between the V and G terms (R^2 = -0.77). When retaining only the five Abraham descriptors in the model calculation, the *v* term is significant and positive, although small, indicating that the retention of large molecules is favoured by (i) interaction with the aromatic rings (dispersive or CH-π interactions), or (ii) to a lesser extent, dispersive interactions with the alkyl spacer arm linking the chiral selector to the silica surface. For instance, increasing alkyl chain length, which is inducing increasing V values while all other molecular descriptors remain virtually constant, is causing a slight increase in retention. Typically, this can be observed in the alkylbenzene series (analytes #2 to #15 in Table S1), phenylalcohol series (analytes #70 to #72),

alkylphenone series (analytes #80 to #82), alkylbenzoate series (analytes #152 to #155), dialkylphthalate series (analytes #156 to #159), and parabens (analytes #160 to #163). Finally, flexibility (described by F descriptor) has no influence on retention neither. It was never observed to have an influence on retention on the other CSPs previously tested [34–38], but is retained in the model for its possible contribution to enantiorecognition.

4.2. Enantioseparation capabilities

Because the two stationary phases were observed to be most similar in their retention and separation behaviour, only the results for the Whelk-O1 phase will be detailed in the following.

In previous works, we have had several occasions to demonstrate a strategy to explain enantioseparation mechanisms with discriminant analyses (DA). Discriminant analysis is a supervised method: the samples (in the present case the racemates) are first classified into two sets of classes (i) based on experimental retention compared to predicted retention (eluted earlier *vs*. later than predicted), or (ii) based on enantioselectivity ($\alpha = 1$ *vs*. $\alpha > 1$). The first set of DA classes is based on experimental retention factors measured for the two enantiomers and comparing these experimental values to the retention factor predicted by Eq. (1), with the models calculated above based on the retention of achiral analytes (Table 1). Because the descriptors are identical for the two enantiomers, there is only one predicted retention factor for each racemate. Usually, both enantiomers appear to be either less retained than predicted, or more retained than predicted, with one of them being close to the predicted value. In rare cases, the first eluted enantiomer is less retained than predicted while the second eluted enantiomer is more retained than predicted. We then have divided the whole set of racemates (see DA classes in Table S2) into two classes: the “early-eluting racemates” and the “late-eluting racemates”. Discriminant analysis applied to the whole set of racemates, using their molecular descriptors as variables and the two classes thus defined is yielding Figure 4a for Whelk-O1. The AUC (area under the ROC curve, which can be observed in supplementary information Figure S1) was 0.829, indicating that the classification obtained is statistically significant. Because there are only two classes, a single axis is sufficient to represent 100% of the variance. On Figure 4a, the structural features that point to the left of the figure have larger descriptor values in the racemates eluting earlier than predicted, while the structural features that point to the right of the figure have larger descriptor values in the racemates eluting later than predicted.

The size and shape features are all significant and can be explained as follows: the late-eluting racemates are mostly small (molecular volume V is pointing to the left) and spherical (globularity G is pointing to the right).The chiral ligand in these stationary phases is known to form a semi-rigid cleft [8]. A large and flat or rod-like molecule (with small sphericity) is unlikely to fit in the chiral cleft but may still be retained (and even resolved) through interactions outside the cleft [46]. For instance, docking studies from Zhao and co-workers [9,10] and from Roussel group [8] showed how the dinitrobenzyl ring could rotate to interact with an analyte that would mostly remain outside the cleft. On the contrary, a small spherical molecule is likely to better fit the walls of the chiral cleft and interact favourably with the different groups of the ligand, favouring stronger retention. This hypothesis is also supported by the observation that nearly all late-eluting racemates (25% of the complete set) showed some enantiorecognition ($\alpha > 1$). In other words, when the enantiomers were favourably included in the chiral cleft, some resolution occurred nearly systematically (19 cases out of 20) for this probe set. Metoprolol was the sole exception in this group. The “early-eluting” racemates, supposedly not included in the chiral cleft, showed much lower success rates with about 50% enantiodiscrimination observed.

We may also note that most acidic species, bearing some anionic charge in the present operating conditions, also belong to this class of late-eluting racemates (D^- is pointing to the right of the figure). This may be surprising since there are no ion-exchange interaction site bearing a permanent charge in this stationary phase. There are however possible residual silanol groups at the silica surface and the two aromatic groups of the chiral selector, which are electron-rich (tetrahydrophenanthrene) and electron-deficient (dinitrobenzene). Residual silanol groups should exert ionic repulsion to anionic analytes, as suggested from the LSER models (negative d^- term). Repulsive interactions with the supporting phase may however be favourable to interaction with the bonded chiral selector, as the analytes would be preferentially retained on the chiral selector rather than penetrating deeper in the stationary phase, thereby promoting enantioseparation. It was also shown [47] in previous molecular modelling studies on Whelk-O1 that non-enantiospecific interactions could influence the way the analytes were interacting with the chiral selector, thereby influencing the enantiorecognition process. In addition, a negatively charged analyte and the π-accceptor dinitrobenzyl ring of the chiral ligand may interact through anion-π interaction [48]. Such interaction may be favoured by the relative flexibility of the dinitrobenzyl ring, which was observed to adapt its torsion angle to favour analyte binding [8,10]. Further molecular modelling studies would be necessary to support any of these hypotheses.

The second set of DA classes examined is based on the enantioselectivity. Any racemate where some enantioseparation is observed ($\alpha > 1$) is classified as “separated” while $\alpha = 1$

would be classified as “non-separated”. Processing the whole data set in one discriminant analysis is possible and is yielding reasonably good statistics in this case (AUC = 0.782, see supplementary information Figure S1). The result can be observed in Figure 4b. However, as we have had occasions to demonstrate in the past [34,35], it is beneficial to use the above early/late-eluting classifiers prior to the DA calculation, because different groups of analytes may be resolved for different reasons. As mentioned above, all (but one) racemates eluting later than predicted were “separated”, thus no DA can be computed specifically for this group as a sufficient number of negative cases are required to obtained statistically meaningful results. The group of early-eluting racemates however was still large, comprising 59 racemates among which 30 were “not separated” and 29 were “separated”. This is a reasonably large and balanced data set to compute a DA, as the number of analytes is nealy equal in each class. The result was statistically significant (AUC = 0.775, see Figure S1 in supplementary information) and presented in Figure 4c. From this figure, we can note that, when the racemates were early-eluting, even if they were mostly large (V pointing to the right) and flat (or rod-like, G pointing to the left) as was defined in the early/late-eluting DA, they could still be separated if they had π electrons to interact with the aromatic rings of the chiral selector (E pointing to the right), dipoles to interact with the nitro groups or amide group of the chiral selector (S pointing to the right) and electron-donating capability to form hydrogen bonds with the –NH- group in the amide function (B pointing to the right). The significant contribution of E, S, and B for this group is consistent with previous observations [9,10], where molecular modelling indicated that many of the less retained analytes were interacting with the chiral selector through the aromatic groups and through hydrogen bonding with the amide proton. Other features (proton-donor capability A, presence of negative or positive charges D^- and D^+ and flexibility F) were non-significant to explain the differences between the two classes. This does not mean that they do not contribute to any interactions but only that they were not sufficiently different between the two classes. For instance, proton-donors (*a* term) and cationic species (d^+ term) were retained (according to LSER model in Figure 3) but they were present equally in both racemate classes (“separated” and “non-separated”). As a result the A term and D^+ term are both close to zero in the discriminant analysis (Figure 4c). The non-discriminant contribution of A term is consistent with the observed orientation of the carbonyl group towards the exterior of the chiral cleft [5], and is also consistent with previous molecular modelling studies, where hydrogen bonding between an analyte proton and the carbonyl or nitro functions of the chiral selector were observed to be much less frequent than the hydrogen bonding to the amide proton [8–10]. The interactions with cationic species could result from the presence of non-bonded silanol groups, which should also be non-enantioselective, or from interactions with the two aromatic groups (tetrahydrophenantrenyl and dinitrobenzyl), as mentioned in the

description of retention models. Most anionic species were included in the late-eluting class thus this feature (D^-) could not be evaluated in the early-eluting class where most analytes had zero D^- value.

Finally, it is interesting to note that flexibility (F term) was non-discriminant. This is rather surprising because flexibility was found to be very significant as an unfavourable feature to enantiorecognition with other CSPs previously characterized, particularly with polysaccharide CSPs and *Cinchona*-based brush-type CSPs [38]. Flexibility is usually deleterious to enantiorecognition because flexible molecules have more conformers, that make the two enantiomers less easily discriminated. Also, as pointed out by Lämmerhofer [49], rigid molecules require less interactions to achieve enantioselectivity as they meet the geometrical requirements easier than flexible molecules. From the discriminant analyses presented here, this is clearly not an issue on these Pirkle-type CSPs. The supposedly negative effects of flexibility may be contradicted by a positive dynamic fit, whereby the interactions between the flexible analytes and the ligand are favoured by conformational adaptation. It is possible that this flexible adaptation of the analyte would be facilitated by the semi-rigid structure of the chiral selector in this Pirkle-type phase, compared to more flexible CSPs (like those based on polysaccharides).

Considering all information from the retention models and discriminant analyses, Figure 5 provides another look at the retention and separation data, in conjunction with structural features. Figure 5 is plotting log α between the two enantiomers versus log *k* of the first eluted enantiomer. Each point thus represents one racemate, while the bubble size is reflecting one structural feature. For instance, π-electrons (E), dipoles (S), sphericity (G) and cationic charges (D^+) are represented. On the top figures, it appears that the smallest values of E and S (small bubbles) are associated to small retention factors (in accordance with the retention models in Figure 3) and small separation factors (in accordance with Figure 4c). In the top right corner of these figures, the bigger bubbles indicate that the molecules that are π-electron-rich (large E values) and/or possess strong dipoles (large S values) have both strong retention and large enantioresolution. According to the observations in Figure 4, these may belong to the late-eluting class, if they are rather small (small V value), spherical (large G value) and possess negative charges (non-zero D^- value) through acidic functions. Typical examples are 2-phenylbutyric acid (analyte #2 in Table S2) and 2-phenylpropionic acid (#3). In addition, enantiomers with large E and/or S features and successful enantioseparation may also belong to the early-eluting class: Figure 4c indicates that favourable enantiorecognition in this case will also depend on the ability to form hydrogen bonds (B term) and the size and shape features, as big (large V value) and flat or rod-like (small G

value) molecules should be favoured. Typical examples are found in the group of β-blockers Acebutolol (analyte #25 in Table S2), Atenolol (#27), Betaxolol (#28), Oxprenolol (#58), Propranolol (#60) and Sotalol (#63). All of them have several heteroatoms with non-binding electrons contributing to large S and B values, and they have long chains inducing both large volume and rod-like shape. Another example is that of benzodiazepines Diazepam (#35), Lorazepam (#49) and Oxazepam (#56) that are all rather large and flat.

However, strong E and S features are not sufficient to achieve enantioseparation, as can be observed with some large bubbles at the bottom line of these figures, corresponding to zero log α values. As mentioned above, no enantioresolution was principally observed in the early-eluting racemates. Thus analytes with large E and S values eluting earlier than expected may still be unresolved, particularly if they are rather small (small V value) and spherical (large G value). Typical examples are found in the group of barbiturates like Glutethimide (#42), Hexobarbital (#43), Secobarbital (#62) and Thiopental (#67): although they have favourable electron and dipole features (E, S and B values), they are all rather small and spherical and remain unresolved.

The bottom left figure in Figure 5 shows that spherical molecules (large G values) are mostly distributed in low retention values (in accordance with Figure 3, indicating exclusion of spherical molecules). However, small spherical molecules (case of “late-eluting racemates”) that are little retained are well separated as appears with positive values of log α on the left of the figure. Again, this would be the case of 2-phenylbutyric and 2-phenylpropionic acids. Non-spherical molecules (flat or rod-like) are more retained and can still be well separated with favourable E, S and B features and a large molecular volume (case of “early-eluting racemates” in Figure 4c). For instance, this is corresponding to the β-blockers and benzodiazepines.

Finally, the case of cationic species is also interesting (bottom right figure). Cations (large D^+ values) are positively retained on this stationary phase (in accordance with Figure 3, indicating favourable retention of cations), thus the large bubbles are mostly on the right side of this figure. However, the presence of cationic charges was non-discriminant to explain enantioseparation (Figure 4b and 4c), thus big bubbles can be found at all levels of α values.

5. Conclusions

Two Pirkle-type chiral stationary phases bearing the same (but enantiomeric) chiral selector from two different manufacturers were characterized for their retention properties through linear solvation energy relationships and for their enantioseparation properties through

discriminant analyses. The two stationary phases appeared to be most similar, with *homeoenergetic* behaviour. π-π interactions were the most significant to explain retention, followed by hydrogen bonding, dipole-dipole interactions and ionic interactions. Steric exclusion was also significant to explain lack of retention for spherical molecules. The racemates possessing favourable features for enantioseparation can be divided into two groups: small spherical molecules that would well fit in the chiral cleft were nearly always resolved, especially is they possessed negative charges. For large and flat or rod-like molecules that are unlikely to fit so well in the chiral cleft, π-π interactions, dipole-dipole interactions and electron-donating properties were most significant to achieve enantioresolution. These observations are in accordance with chemical sense and previous investigations on these chiral selectors.

Acknowledgment

Jelena Kocergin (formerly at Regis Technologies) and Albin Maisch (Dr. Maisch) are acknowledged for the kind gift of a column for this study. CW also thanks the Institut Universitaire de France (IUF), of which she is a junior member, for the support received.

References

[1] F. Gasparrini, D. Misiti, C. Villani, High-performance liquid chromatography chiral stationary phases based on low-molecular-mass selectors, J. Chromatogr. A. 906 (2001) 35–50. https://doi.org/10.1016/S0021-9673(00)00953-5.

[2] J. Haginaka, Protein-based chiral stationary phases for high-performance liquid chromatography enantioseparations, J. Chromatogr. A. 906 (2001) 253–273. https://doi.org/10.1016/S0021-9673(00)00504-5.

[3] V.A. Davankov, Chiral selectors with chelating properties in liquid chromatography: Fundamental reflections and selective review of recent developments, J. Chromatogr. A. 666 (1994) 55–76. https://doi.org/10.1016/0021-9673(94)80370-6.

[4] C.J. Welch, Evolution of chiral stationary phase design in the Pirkle laboratories, J. Chromatogr. A. 666 (1994) 3–26. https://doi.org/10.1016/0021-9673(94)80367-6.

[5] C. Fernandes, M.E. Tiritan, M. Pinto, Small Molecules as Chromatographic Tools for HPLC Enantiomeric Resolution: Pirkle-Type Chiral Stationary Phases Evolution, Chromatographia. 76 (2013) 871–897. https://doi.org/10.1007/s10337-013-2469-8.

[6] L.H. Easson, E. Stedman, Studies on the relationship between chemical constitution and physiological action, Biochem. J. 27 (1933) 1257–1266. https://doi.org/10.1042/bj0271257.

[7] C.E. Dalgliesh, 756. The optical resolution of aromatic amino-acids on paper chromatograms, J. Chem. Soc. Resumed. (1952) 3940. https://doi.org/10.1039/jr9520003940.

[8] A. Del Rio, J.M. Hayes, M. Stein, P. Piras, C. Roussel, Theoretical reassessment of Whelk-O1 as an enantioselective receptor for 1-(4-halogeno-phenyl)-1-ethylamine derivatives, Chirality. 16 (2004) S1–S11. https://doi.org/10.1002/chir.20009.

[9] C.F. Zhao, N.M. Cann, Molecular Dynamics Study of Chiral Recognition for the Whelk-O1 Chiral Stationary Phase, Anal. Chem. 80 (2008) 2426–2438. https://doi.org/10.1021/ac702126y.

[10] C.F. Zhao, S. Diemert, N.M. Cann, Rational optimization of the Whelk-O1 chiral stationary phase using molecular dynamics simulations, J. Chromatogr. A. 1216 (2009) 5968–5978. https://doi.org/10.1016/j.chroma.2009.06.041.

[11] M.E. Koscho, P.L. Spence, W.H. Pirkle, Chiral recognition in the solid state: crystallographically characterized diastereomeric co-crystals between a synthetic chiral selector (Whelk-O1) and a representative chiral analyte, Tetrahedron Asymmetry. 16 (2005) 3147–3153. https://doi.org/10.1016/j.tetasy.2005.08.027.

[12] B. Chankvetadze, Recent developments on polysaccharide-based chiral stationary phases for liquid-phase separation of enantiomers, J. Chromatogr. A. 1269 (2012) 26–51. https://doi.org/10.1016/j.chroma.2012.10.033.

[13] G.K.E. Scriba, Chiral recognition in separation sciences. Part I: Polysaccharide and cyclodextrin selectors, TrAC Trends Anal. Chem. 120 (2019) 115639. https://doi.org/10.1016/j.trac.2019.115639.

[14] J. Shen, Y. Okamoto, 8.11 Chromatographic Separations and Analysis: Cellulose and Polysaccharide Derivatives as Stationary Phases, in: Compr.

Chirality, Elsevier, 2012: pp. 200–226. https://doi.org/10.1016/B978-0-08-095167-6.00824-7.
[15] G.K.E. Scriba, Chiral recognition in separation sciences. Part II: Macrocyclic glycopeptide, donor-acceptor, ion-exchange, ligand-exchange and micellar selectors, TrAC Trends Anal. Chem. 119 (2019) 115628. https://doi.org/10.1016/j.trac.2019.115628.
[16] I. Ilisz, R. Berkecz, A. Péter, Retention mechanism of high-performance liquid chromatographic enantioseparation on macrocyclic glycopeptide-based chiral stationary phases, J. Chromatogr. A. 1216 (2009) 1845–1860. https://doi.org/10.1016/j.chroma.2008.08.041.
[17] A. Berthod, 8.12 Chromatographic Separations and Analysis: Macrocyclic Glycopeptide Chiral Stationary Phases, in: Compr. Chirality, Elsevier, 2012: pp. 227–262. https://doi.org/10.1016/B978-0-08-095167-6.00825-9.
[18] W.H. Pirkle, C.J. Welch, Use of simultaneous face to face and face to edge π-π interactions to facilitate chiral recognition, Tetrahedron Asymmetry. 5 (1994) 777–780. https://doi.org/10.1016/S0957-4166(00)86225-4.
[19] E.R. Francotte, Enantioselective chromatography as a powerful alternative for the preparation of drug enantiomers, J. Chromatogr. A. 906 (2001) 379–397. https://doi.org/10.1016/S0021-9673(00)00951-1.
[20] E. Badaloni, W. Cabri, A. Ciogli, R. Deias, F. Gasparrini, F. Giorgi, A. Vigevani, C. Villani, Combination of HPLC “Inverted Chirality Columns Approach” and MS/MS Detection for Extreme Enantiomeric Excess Determination Even in Absence of Reference Samples. Application to Camptothecin Derivatives, Anal. Chem. 79 (2007) 6013–6019. https://doi.org/10.1021/ac070776j.
[21] E. Badaloni, W. Cabri, A. Ciogli, I. D’Acquarica, R. Deias, F. Gasparrini, F. Giorgi, D. Kotoni, C. Villani, Extending the use of “Inverted Chirality Columns Approach” for enantiomeric excess determination in absence of reference samples: Application to a water-soluble camptothecin derivative, J. Chromatogr. A. 1217 (2010) 1024–1032. https://doi.org/10.1016/j.chroma.2009.10.035.
[22] G. Mazzoccanti, O.H. Ismail, I. D’Acquarica, C. Villani, C. Manzo, M. Wilcox, A. Cavazzini, F. Gasparrini, Cannabis through the looking glass: chemo- and enantio-selective separation of phytocannabinoids by enantioselective ultra high performance supercritical fluid chromatography, Chem. Commun. 53 (2017) 12262–12265. https://doi.org/10.1039/C7CC06999E.
[23] L. Sciascera, O. Ismail, A. Ciogli, D. Kotoni, A. Cavazzini, L. Botta, T. Szczerba, J. Kocergin, C. Villani, F. Gasparrini, Expanding the potential of chiral chromatography for high-throughput screening of large compound libraries by means of sub–2μm Whelk-O 1 stationary phase in supercritical fluid conditions, J. Chromatogr. A. 1383 (2015) 160–168. https://doi.org/10.1016/j.chroma.2015.01.042.
[24] O.H. Ismail, G.L. Losacco, G. Mazzoccanti, A. Ciogli, C. Villani, M. Catani, L. Pasti, S. Anderson, A. Cavazzini, F. Gasparrini, Unmatched Kinetic Performance in Enantioselective Supercritical Fluid Chromatography by Combining Latest Generation Whelk-O1 Chiral Stationary Phases with a Low-Dispersion in-House Modified Equipment, Anal. Chem. 90 (2018) 10828–10836. https://doi.org/10.1021/acs.analchem.8b01907.
[25] C.J. Welch, M. Biba, J.R. Gouker, G. Kath, P. Augustine, P. Hosek, Solving multicomponent chiral separation challenges using a new SFC tandem column screening tool, Chirality. 19 (2007) 184–189. https://doi.org/10.1002/chir.20357.

[26] E. Lesellier, C. West, The many faces of packed column supercritical fluid chromatography - A critical review, J. Chromatogr. A. 1382 (2015) 2–46. https://doi.org/10.1016/j.chroma.2014.12.083.
[27] C. West, Current trends in supercritical fluid chromatography, Anal. Bioanal. Chem. 410 (2018) 6441–6457. https://doi.org/10.1007/s00216-018-1267-4.
[28] C. West, Enantioselective Separations with Supercritical Fluids - Review, Curr. Anal. Chem. 10 (2014) 99–120. https://doi.org/10.2174/1573411011410010009.
[29] C. West, Recent trends in chiral supercritical fluid chromatography, TrAC Trends Anal. Chem. 120 (2019) 115648. https://doi.org/10.1016/j.trac.2019.115648.
[30] S. Khater, M.-A. Lozac'h, I. Adam, E. Francotte, C. West, Comparison of liquid and supercritical fluid chromatography mobile phases for enantioselective separations on polysaccharide stationary phases, J. Chromatogr. A. 1467 (2016) 463–472. https://doi.org/10.1016/j.chroma.2016.06.060.
[31] R.W. Stringham, Relationship between resolution and analysis time in chiral subcritical fluid chromatography, Chirality. 8 (1996) 249–257. https://doi.org/10.1002/(SICI)1520-636X(1996)8:3<249::AID-CHIR4>3.0.CO;2-C.
[32] C. West, Y. Zhang, L. Morin-Allory, Insights into chiral recognition mechanisms in supercritical fluid chromatography. I. Non-enantiospecific interactions contributing to the retention on tris-(3,5-dimethylphenylcarbamate) amylose and cellulose stationary phases, J. Chromatogr. A. 1218 (2011) 2019–2032. https://doi.org/10.1016/j.chroma.2010.11.084.
[33] C. West, G. Guenegou, Y. Zhang, L. Morin-Allory, Insights into chiral recognition mechanisms in supercritical fluid chromatography. II. Factors contributing to enantiomer separation on tris-(3,5-dimethylphenylcarbamate) of amylose and cellulose stationary phases, J. Chromatogr. A. 1218 (2011) 2033–2057. https://doi.org/10.1016/j.chroma.2010.11.085.
[34] S. Khater, Y. Zhang, C. West, Insights into chiral recognition mechanism in supercritical fluid chromatography III. Non-halogenated polysaccharide stationary phases, J. Chromatogr. A. 1363 (2014) 278–293. https://doi.org/10.1016/j.chroma.2014.06.084.
[35] S. Khater, Y. Zhang, C. West, Insights into chiral recognition mechanism in supercritical fluid chromatography IV. Chlorinated polysaccharide stationary phases, J. Chromatogr. A. 1363 (2014) 294–310. https://doi.org/10.1016/j.chroma.2014.06.026.
[36] S. Khater, C. West, Characterization of three macrocyclic glycopeptide stationary phases in supercritical fluid chromatography, J. Chromatogr. A. 1604 (2019) 460485. https://doi.org/10.1016/j.chroma.2019.460485.
[37] A. Raimbault, C. West, Effects of high concentrations of mobile phase additives on retention and separation mechanisms on a teicoplanin aglycone stationary phase in supercritical fluid chromatography, J. Chromatogr. A. 1604 (2019) 460494. https://doi.org/10.1016/j.chroma.2019.460494.
[38] A. Raimbault, C.M.A. Ma, M. Ferri, S. Bäurer, P. Bonnet, S. Bourg, M. Lämmerhofer, C. West, Cinchona-based zwitterionic stationary phases: Exploring retention and enantioseparation mechanisms in supercritical fluid chromatography with a fragmentation approach, J. Chromatogr. A. 1612 (2020) 460689. https://doi.org/10.1016/j.chroma.2019.460689.
[39] S. Khater, Y. Zhang, C. West, In-depth characterization of six cellulose tris-(3,5-dimethylphenylcarbamate) chiral stationary phases in supercritical fluid

chromatography, J. Chromatogr. A. 1303 (2013) 83–93. https://doi.org/10.1016/j.chroma.2013.06.040.
[40] C. West, E. Lemasson, S. Khater, E. Lesellier, An attempt to estimate ionic interactions with phenyl and pentafluorophenyl stationary phases in supercritical fluid chromatography, J. Chromatogr. A. 1412 (2015) 126–138. https://doi.org/10.1016/j.chroma.2015.08.009.
[41] K.B. Lipkowitz, Theoretical studies of brush-type chiral stationary phases, J. Chromatogr. A. 666 (1994) 493–503. https://doi.org/10.1016/0021-9673(94)80411-7.
[42] R. Sheridan, W. Schafer, P. Piras, K. Zawatzky, E.C. Sherer, C. Roussel, C.J. Welch, Toward structure-based predictive tools for the selection of chiral stationary phases for the chromatographic separation of enantiomers, J. Chromatogr. A. 1467 (2016) 206–213. https://doi.org/10.1016/j.chroma.2016.05.066.
[43] W. Melander, J. Stoveken, C. Horváth, Stationary phase effects in reversed-phase chromatography, J. Chromatogr. A. 199 (1980) 35–56. https://doi.org/10.1016/S0021-9673(01)91360-3.
[44] R. Dallocchio, A. Dessì, M. Solinas, A. Arras, S. Cossu, E. Aubert, V. Mamane, P. Peluso, Halogen bond in high-performance liquid chromatography enantioseparations: Description, features and modelling, J. Chromatogr. A. 1563 (2018) 71–81. https://doi.org/10.1016/j.chroma.2018.05.061.
[45] W.F. Baitinger, P. von R. Schleyer, T.S.S.R. Murty, L. Robinson, Nitro groups as proton acceptors in hydrogen bonding, Tetrahedron. 20 (1964) 1635–1647. https://doi.org/10.1016/S0040-4020(01)99161-6.
[46] M.E. Koscho, W.H. Pirkle, Investigation of a broadly applicable chiral selector used in enantioselective chromatography (Whelk-O 1) as a chiral solvating agent for NMR determination of enantiomeric composition, Tetrahedron Asymmetry. 16 (2005) 3345–3351. https://doi.org/10.1016/j.tetasy.2005.08.032.
[47] A. Knežević, J. Novak, V. Vinković, New Brush-Type Chiral Stationary Phases for Enantioseparation of Pharmaceutical Drugs, Molecules. 24 (2019) 823. https://doi.org/10.3390/molecules24040823.
[48] P. Gamez, T.J. Mooibroek, S.J. Teat, J. Reedijk, Anion Binding Involving π-Acidic Heteroaromatic Rings, Acc. Chem. Res. 40 (2007) 435–444. https://doi.org/10.1021/ar7000099.
[49] M. Lämmerhofer, Chiral recognition by enantioselective liquid chromatography: Mechanisms and modern chiral stationary phases, J. Chromatogr. A. 1217 (2010) 814–856. https://doi.org/10.1016/j.chroma.2009.10.022.

686 **Figure Caption**

687

688 **Figure 1**. Structure of the chiral selector in the (R,R)-Whelk-O1 stationary phase and
689 features of the different fragments of the chiral selector. The ligand in ReproSil
690 Chiral-NR is the (S,S) enantiomer of this one.

691

692 **Figure 2**. Scattergrams and box-plots of (a) retention factors for the 212 achiral
693 analytes in Table S1 and (b) separation factors for the 79 racemates in Table S2 on
694 (R,R)-Whelk-O1. Chromatographic conditions: CO_2-methanol 90:10 (v/v), 25°C, 15
695 MPa, 3 mL/min.

696

697 **Figure 3**. Histogram representing normalized coefficients of the LSER model
698 calculated with the retention data measured for the 212 analytes in Table S1 and Eq.
699 (1) on the (R,R)-Whelk-O1 column (left bars) and ReproSil Chiral-NR column (right
700 bars). Error bars indicate the 95% confidence limits. Chromatographic conditions:
701 see Figure 2.

702

703 **Figure 4.** Discriminant analyses using nine molecular descriptors as variables and
704 the 79 racemates eluted from (R,R)-Whelk-O1 in Table S2.
705 (a) Discrimination between early-eluting (left) and late-eluting (right) racemates
706 indicating the structural features favouring some form of exclusion from the stationary
707 phase (left) or inclusion (right).
708 (b) & (c) Discrimination between non-separated (left) and separated (right) racemates
709 where negative features are common to the racemates that were not separated on
710 this stationary phase and positive features are common to separated racemates. (b)
711 including all racemates (c) including only early-eluting racemates.
712 Chromatographic conditions: see Figure 2.

713

714 **Figure 5.** Bubble graphs to compare retention and separation values for the chiral
715 analytes in Table S2 depending on their structural features. Large bubbles indicate
716 large values for each molecular descriptor.
717 Chromatographic conditions : see Figure 2.

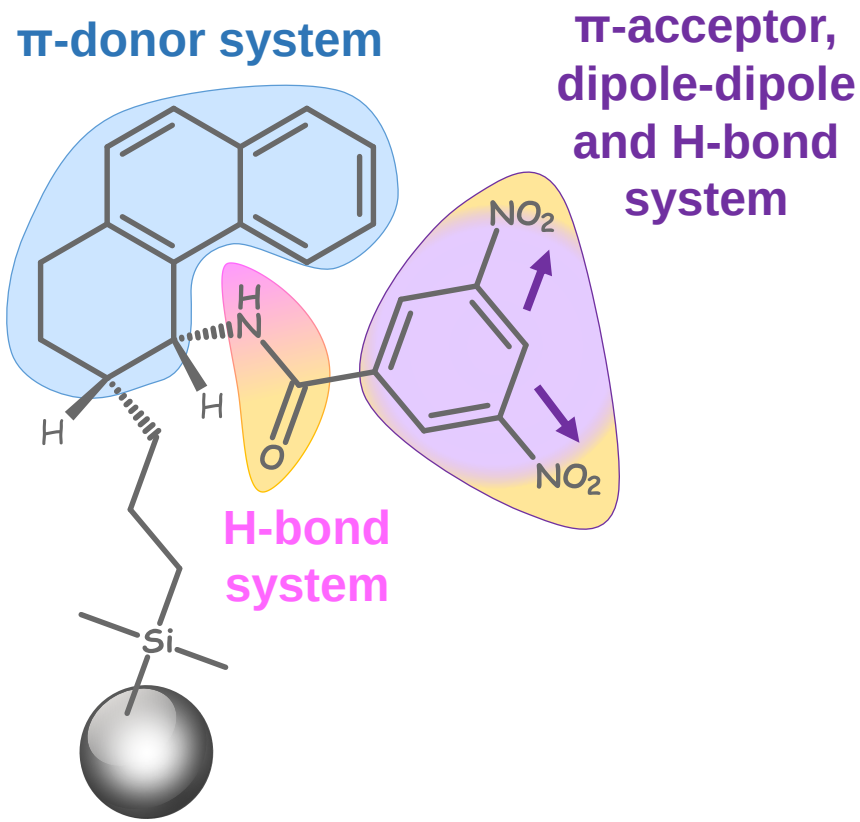

Figure 1: Structure of the chiral selector in the (R,R)-Whelk-O1 stationary phase and features of the different fragments of the chiral selector. The ligand in ReproSil Chiral-NR is the (S,S) enantiomer of this one.

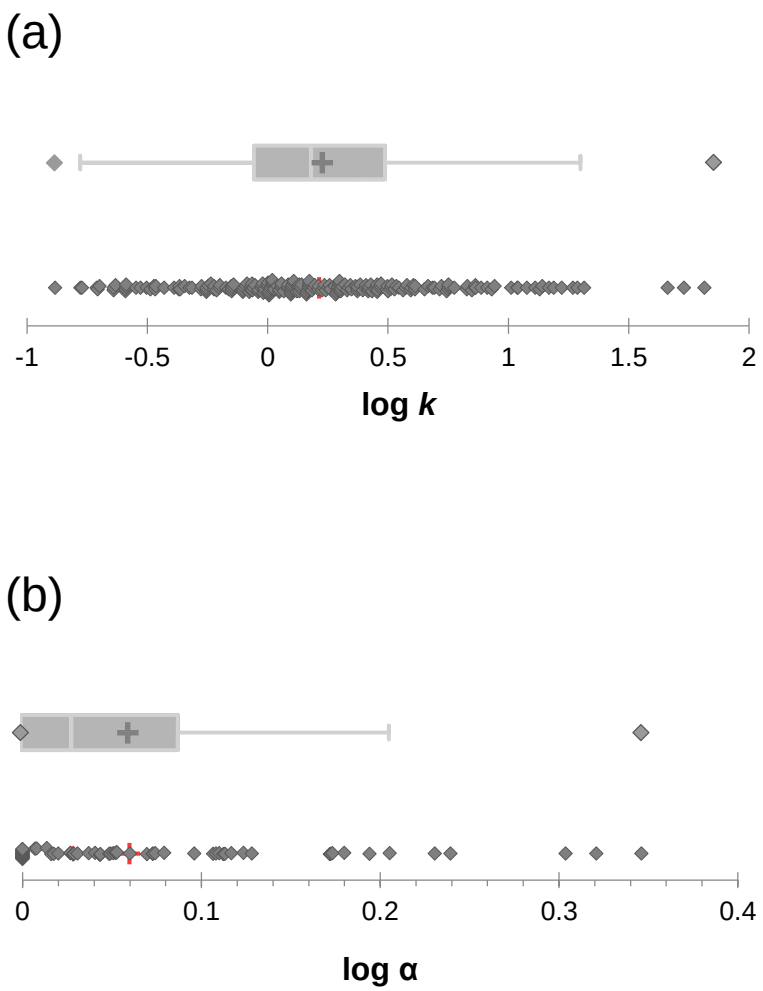

Figure 2: Scattergrams and box-plots of (a) retention factors for the 212 achiral analytes in Table S1 and (b) separation factors for the 79 racemates in Table S2 on (R,R)-Whelk-O1. Chromatographic conditions: CO_2-methanol 90:10 (v/v), 25°C, 15 MPa, 3 mL/min.

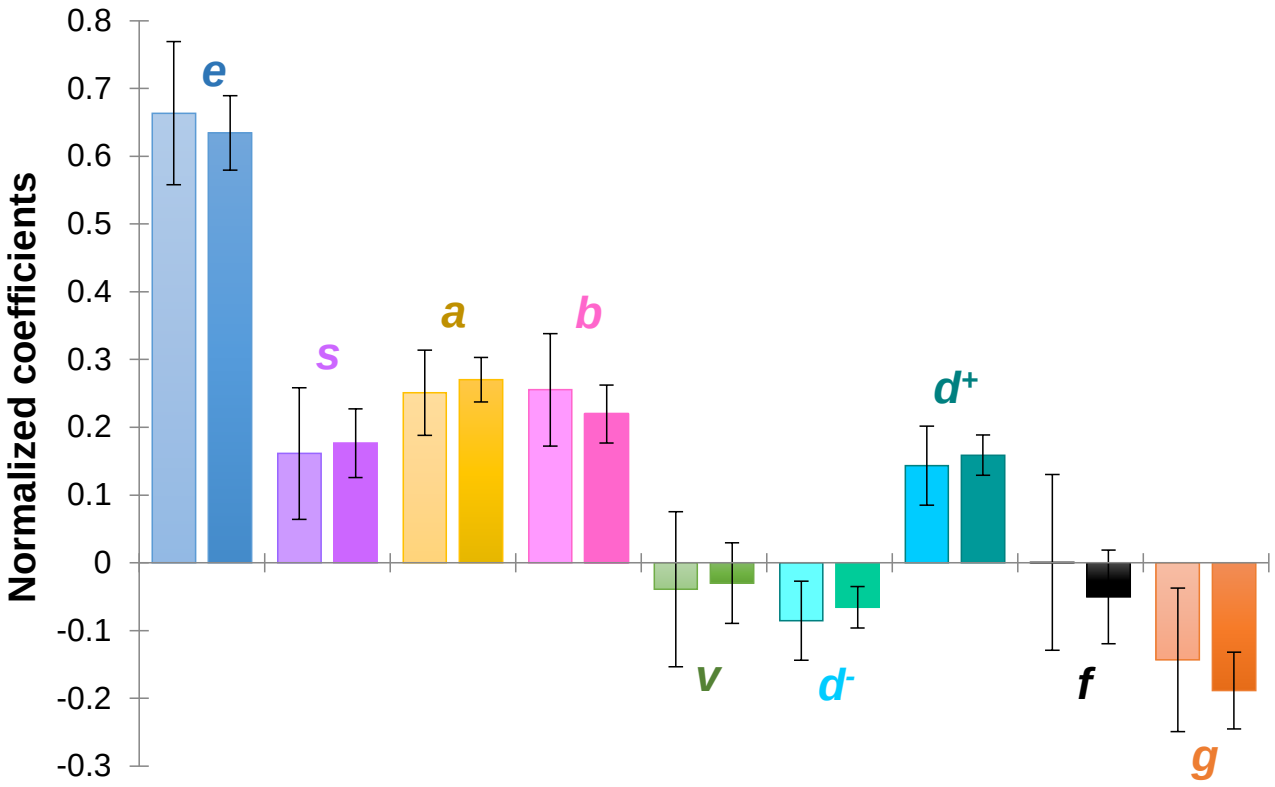

Figure 3: Histogram representing normalized coefficients of the LSER model calculated with the retention data measured for the 212 analytes in Table S1 and Eq. (1) on the Whelk-O1 column (left bars) and Reprosil Chiral-NR column (right bars). Error bars indicate the 95% confidence limits. Chromatographic conditions: see Figure 2.

Figure 4: Discriminant analyses using nine molecular descriptors as variables and the 79 racemates eluted from (R,R)-Whelk-O1 in Table S2.
(a) Discrimination between early-eluting (left) and late-eluting (right) racemates indicating the structural features favouring some form of exclusion from the stationary phase (left) or inclusion (right).
(b) & (c) Discrimination between non-separated (left) and separated (right) racemates where negative features are common to the racemates that were not separated on this stationary phase and positive features are common to separated racemates. (b) including all racemates (c) including only early-eluting racemates.

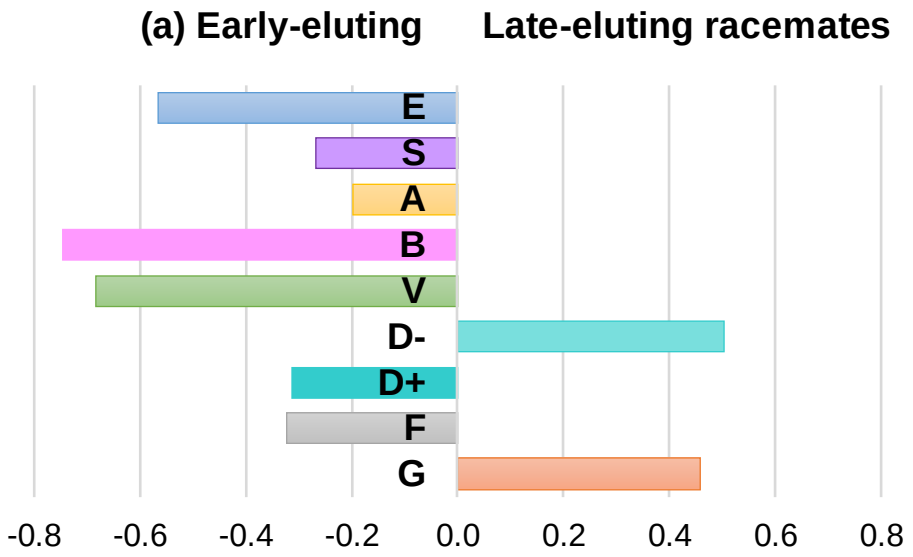

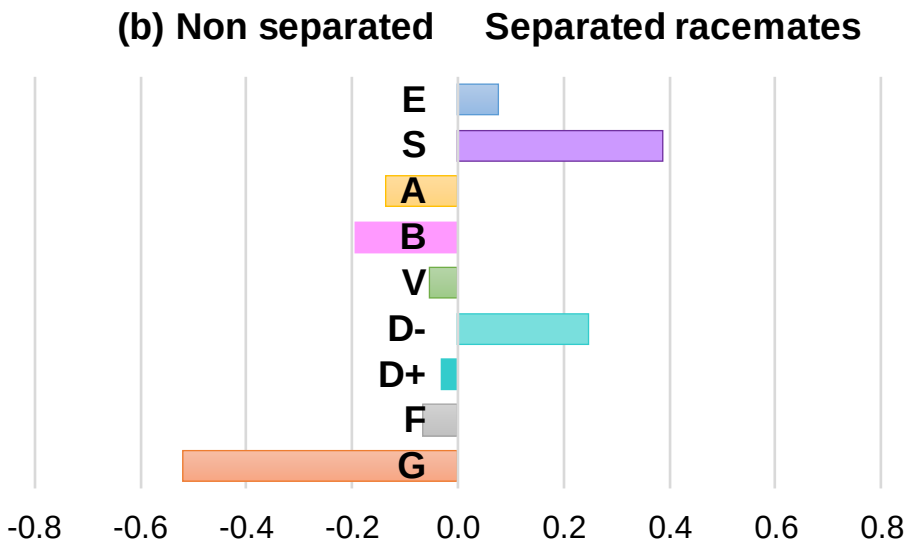

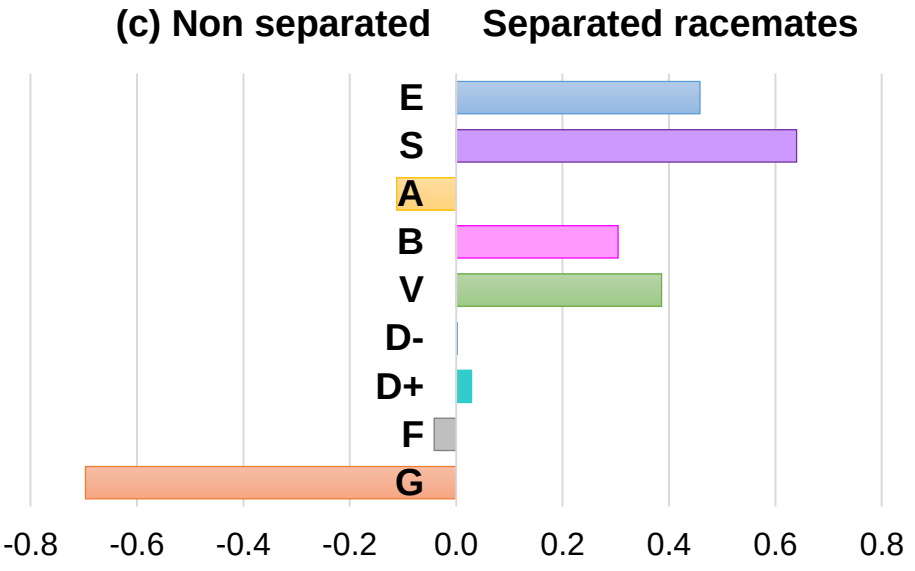

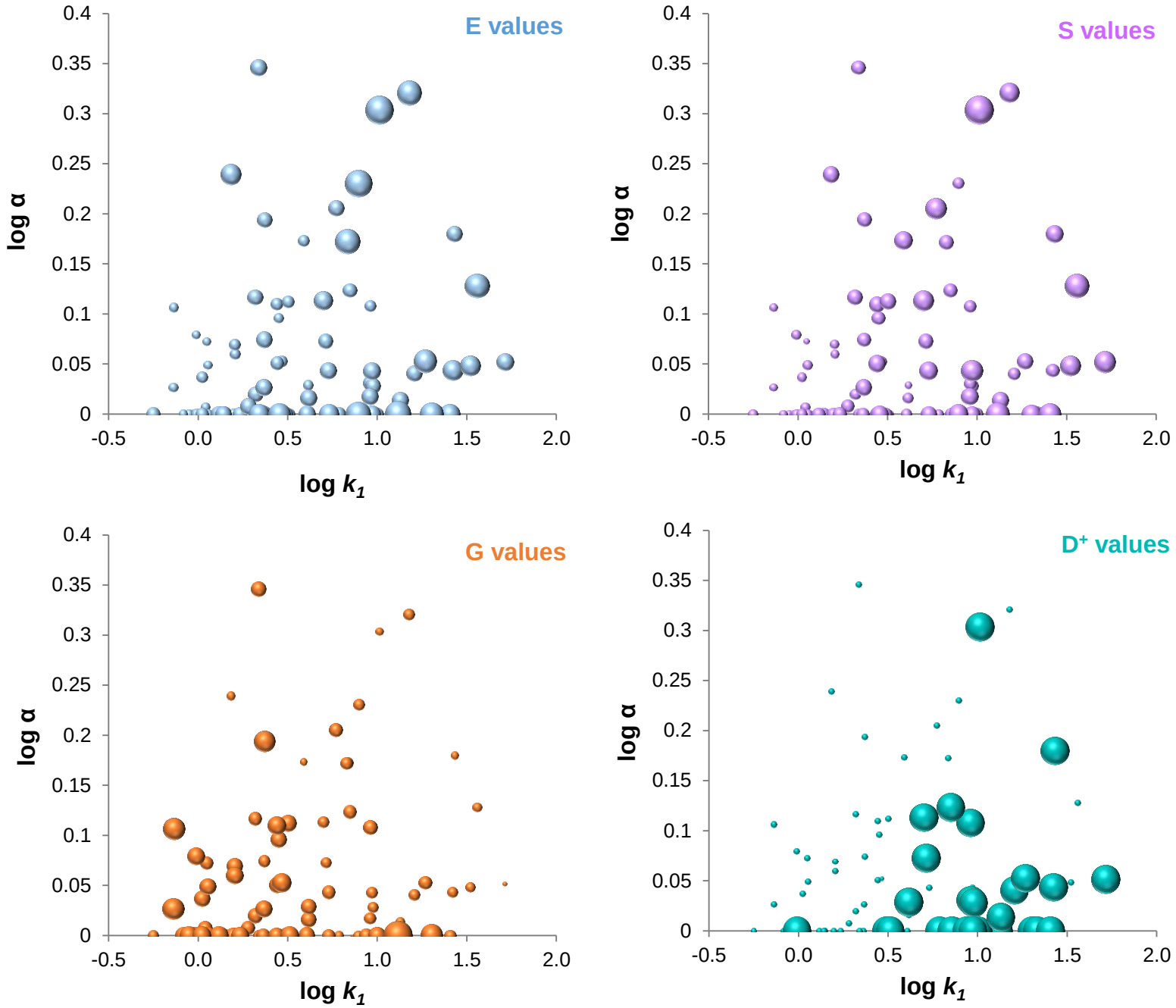

Figure 5: Bubble graphs to compare retention and separation values for the chiral analytes in Table S2 depending on their structural features. Large bubbles indicate large values for each molecular descriptor.

Table 1 system constants and statistics for the 2 columns tested
obtained with Eq.(1), with or without additive in the mobile phase
n is the number of solutes finally retained in the multiple linear regression;
R^2_{adj} is the adjusted determination coefficient; *SE* in the standard error in the estimate

Column	*c*	*e*	*s*	*a*	*b*	*v*	d^-	d^+	*f*	*g*	n	R^2_{adj}	*SE*
Whelk-O1	-0.640	0.598	0.184	0.361	0.413	-0.039	-0.137	0.258	0.000	-0.190	212	0.856	0.280
	0.167	*0.048*	*0.056*	*0.046*	*0.068*	*0.058*	*0.047*	*0.053*	*0.036*	*0.071*			
ReproSil Chiral-NR	-0.413	0.462	0.159	0.307	0.284	-0.024	-0.081	0.259	-0.021	-0.195	200	0.854	0.142
	0.136	*0.040*	*0.045*	*0.037*	*0.055*	*0.047*	*0.038*	*0.049*	*0.030*	*0.058*			